Design of 600 W Low Loss Ultra-wideband Ferriteless Balun

Chi Van Pham, *Student Member, IEEE*, Anh-Vu Pham, *Senior Member, IEEE*, and Robert E. Leoni III *Member, IEEE*

***Abstract*—We present the development of a low loss, high power, and ferriteless balun that operates over 0.1-1.6 GHz bandwidth. The proposed balun employs a novel compensated circuit, a single quarter-wave semi-rigid coaxial cable and an on-board inductor on a thermoset ceramic board to achieve high power and ultra-wide bandwidth performance. The experimental results show that the balun achieves a measured average insertion loss of less than 0.5 dB and return loss of better than 10 dB from 100 MHz to more than 1.6 GHz. Within the measured bandwidth, the amplitude and phase imbalances are within ±1 dB and ±5°, respectively. Multiphysics analysis and high power measurements demonstrate that the balun can handle more than 600 W and above at 1.6 GHz. To the best of our knowledge, the reported balun has the highest measured power handling capability per the largest 16:1 bandwidth ratio to date.**

***Index Terms*—Transmission line balun, wide bandwidth balun, defected ground structure, semi-rigid coaxial cable, multiphysics analysis, power handling capability.**

I. Introduction

HIGH power, wide bandwidth, low-loss and compact baluns with an average power handling capability of more than 500 W are used in push-pull amplifiers for wireless base stations, broadcast transmitters, air traffic control systems, and multi-functional radar systems [1]-[4]. Marchand compensated transmission line concepts [5]-[12] are widely used to design wide bandwidth baluns on printed circuit boards. Other techniques including parallel and serial-connected coaxial lines [13]-[18], ferrite coupled-coil lines [19], [20] and coaxial lines loaded with bulky ferrite cores [21] have been used to extend the balun bandwidth. Phelan [13] and Robert [14] connected a single coaxial section with another short parallel solid rod and serial coaxial transmission line to obtain a good input matching over two widely-separated frequencies. Dunn [16] machined coaxial cables to have a larger characteristic impedance of the coaxial line to achieve a 13:1 bandwidth ratio. Note that these baluns have at least two λ/4 coaxial sections to maintain symmetry at balanced ports. Their sizes become excessively large at low frequencies. To operate at low frequencies down to a few MHz's, a typical coaxial balun loads its λ/4 coaxial line with ferrite beads that enhance the inductance per unit length, consequently increasing the characteristic impedance of the coaxial transmission line [21]-[23]. Coupled-wire baluns are formed by winding a coaxial cable in N turns to enhance inductance by a factor N^2, resulting in a very large balun structure [19], [20]. Recently, to realize a compact size and broadband performance, multilayered planar baluns employing defected ground structures have been proposed but only operated at low power levels [6], [9]. While the multilayered baluns in [6]-[10] achieve broadband and low-loss performance, they are not suitable for high power applications because those balun topologies use broadside coupled transmission lines. The broadside coupled-line on multilayered thin-films have small trace width and a narrow gap (25 to 50 μm) between the top and bottom conductors for tight coupling. The small gap required to achieve electrical performance suffers high electric field breakdown in high power applications [24].

High power and wide bandwidth baluns employing ferrite cores have been reported for CW-signals smaller than 200 W power between 0.1 to 2 GHz [19]-[23]. In these baluns, a ferrite core with high permeability is used with a conventional quarter-wavelength transmission line to convert a single-ended signal into a balanced one. The power handling capabilities of the ferrite baluns [21]-[23] are limited by the ferrite materials that suffer high losses and magnetic saturation [25]. The ferrite, dielectric and conductive losses produce internal heat that contributes to the circuit breakdown of the coaxial baluns [24], [26], [27]. The power handling capability also depends on the glass transition temperature of the substrate material and coaxial dielectric [28], [29]. Ferriteless baluns [3], [4] with power handling capabilities from 500 W to 700 W have been reported but have a narrow operating bandwidth. The non-ferrite high-power balun in [4] uses conventional quarter wavelength coaxial cables on ceramic substrates to achieve a bandwidth ratio of 2:1 around a center frequency of 725 MHz. To date, wide bandwidth (above 5:1 bandwidth ratio) and high power handling baluns (more than 500 W) have not been reported. Also, the power handling capability of the coaxial baluns has not been thoroughly investigated.

Manuscript received January 24, 2017; revised June 01, 2017 and August 29, 2017. This work is supported by the Raytheon Company. This document does not contain technology or Technical Data controlled under either the U.S. International Traffic in Arms Regulations or the U.S. Export Administration Regulations.

Chi Van Pham and A.-V. Pham are with the Electrical and Computer Engineering Department, the University of California at Davis, Davis, CA 95616 USA (e-mail: cvpham@ucdavis.edu; pham@ece.ucdavis.edu)

R. E. Leoni III is with Raytheon Company, Integrated Defense Systems, Andover, MA 01810 USA

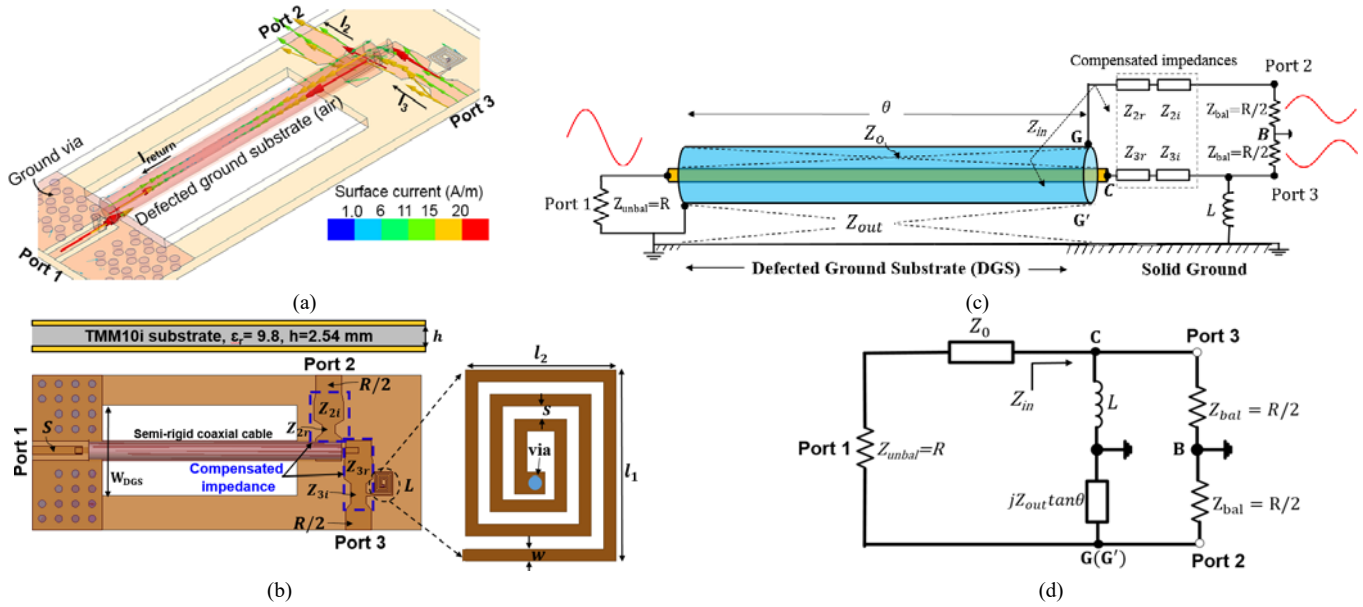

Fig. 1. Proposed wide bandwidth and high power balun. (a) 3-D view with the surface current flow. (b) Cross section and top view. (c) Circuit diagram. (d) Transmission line equivalent circuit without compensated impedances Z_{2r}, Z_{2i}, Z_{3r} and Z_{3i}.

In this paper, we present a modified coaxial balun that can achieve simultaneously ultra-wideband (16:1 bandwidth ratio), low loss, compact and high-power handling of more than 600 W. For the first time, the defected ground structure and the compensated inductor techniques are applied to a high power coaxial-type balun to achieve both wide bandwidth and high power handling capabilities. The balun is implemented using only one quarter-wavelength semi-rigid coaxial cable on a rectangular defected substrate. An on-board inductor and compensated sections are designed to enhance the balun balances and to transform the impedance of balanced ports. The new balun topology avoids the use of broadside coupled-lines having small gaps and solely relies on the ultra-low loss semi-rigid coaxial cable and a high thermal ceramic substrate to form the state-of-the-art 600-W balun. We also report the theoretical and comprehensive multiphysics analysis and characterization of average power handling capabilities, thermal stress, structural integrity and electrical performance of the proposed balun. Finally, we have conducted high power measurements with a thermal infrared camera to validate that the balun can handle up to 600 W at 1.6 GHz without any electrical and structural breakdown.

The paper is structured as follows. Section II of this paper presents the design analysis of the proposed balun. In this section, the balun model and its equivalent circuit are analyzed to develop design procedures and demonstrate electrical performance. This section also provides a study of power handling capabilities of the balun using both theoretical derivation and multiphysics simulations. Section III shows electrical and high power measurements to validate the balun prototype. Finally, the conclusion is presented in Section IV.

II. Design Of The 600 W Ferriteless Balun

A. Balun Operation and Impedance Bandwidth Analysis

Fig. 1 shows the proposed high power and wide bandwidth coaxial transmission line balun, its schematic diagram and an equivalent circuit model. This balun consists of a semi-rigid coaxial cable sitting on a single layer ceramic board with a rectangular-shaped defected ground substrate (DGS). The modified DGS width is W_{DGS} while the coaxial cable has an outer diameter of 6.4 mm and a length of 75 mm provided by Micro-Coax. The characteristic impedance and electrical length of the coaxial transmission line (TL) are denoted as Z_0 and θ, respectively. The balun balanced ports (Ports 2 and 3) have a compensated on-board spiral inductor L at Port 3 and compensated impedances, Z_{2r}, Z_{2i} and Z_{3r}, Z_{3i} for Ports 2 and 3, respectively. As the on-board inductor plays a major role in the impedance bandwidth at very low frequencies, the ideal inductor value is used to derive the bandwidth equation of the balun. When analyzing the imbalances of the balun, however, the self-resonance behavior can affect the phase and amplitude differences over the bandwidth. Therefore, a microstrip inductor model incorporating its self-resonance frequency is used in circuit simulation and analysis.

Fig. 1(a) and (c) show a 3-D cross-section view and circuit diagram of the balun. A traveling wave from Port 1 sees a symmetric path that consists of Port 2, Port 3 and a parasitic transmission line between the coaxial metallic shield and the printed circuit board (PCB) ground plane. Inside the semi-rigid coaxial transmission line, the signal and ground return waves are always out-of-phase, and they each travel down to balanced ports in an odd-mode propagation. At the balanced ports, I_2 and I_3 have the same magnitude but are out of phase to form balanced signals. The symbols $Z_{unbal} = R$ and $Z_{bal} = R/2$ represent the terminating impedance of the unbalanced port and

balanced ports, respectively, while Z_{out} is the characteristic impedance of the parasitic transmission line between the outer conductor of the semi-rigid coaxial cable to the PCB ground. Z_{out} must be much larger than R to minimize current return (I_{return}), resulting in a wide bandwidth impedance match at the unbalanced port. The compensating inductor and impedances (Z_{2r}, Z_{2i}, Z_{3r} and Z_{3i}) improve the balance of the balun, resulting in maximum bandwidth performance.

Using the transmission line equations from [30], the circuit diagram in Fig. 1(c) is simplified as an equivalent circuit in Fig. 1(d) that neglects compensated impedances Z_{2r}, Z_{2i}, Z_{3r}, and Z_{3i}. Considering G′ and G are the same for the sake of drawing the circuit diagram. The impedance looking into G′, which is the transmission line Z_{out} with the other end shorted at Port 1, is $jZ_{out}\tan\theta$. Assuming the transmission line is lossless [11], [30], Z_{in} in Fig. 1(d) can be derived to evaluate the bandwidth of the proposed balun as:

$$Z_{in} = R_{in} + jX_{in} = \frac{(jZ_{out}\tan\theta)\frac{R}{2}}{jZ_{out}\tan\theta + \frac{R}{2}} + \frac{(j\omega L)\frac{R}{2}}{j\omega L + \frac{R}{2}} = Z_1 + Z_2 \quad (1)$$

$$Z_{in} = R_{in} + jX_{in} = \left(\frac{2RZ_{out}^2\tan^2\theta}{R^2 + 4Z_{out}^2\tan^2\theta} + \frac{2R\omega^2L^2}{R^2 + 4\omega^2L^2}\right) + j\left(\frac{R^2Z_{out}\tan\theta}{R^2 + 4Z_{out}^2\tan^2\theta} + \frac{R^2\omega L}{R^2 + 4\omega^2L^2}\right) \quad (2)$$

where $\theta = \pi f/(2f_0)$ and f_0 is a center frequency of the operating bandwidth of the balun. The proposed balun uses a single coaxial section with a length of a quarter-wavelength calculated at $f_0 = 1$ GHz.

Normalizing Z_{in} relative to $R/2$, $z_n = r_n + jx_n = 2Z_{in}/R$ and let $\alpha = 2Z_{out}\tan\theta/R$ and $\beta = 2\omega L/R$, then r_n and x_n are given by,

$$r_n = \frac{2R_{in}}{R} = \frac{\alpha^2}{1+\alpha^2} + \frac{\beta^2}{1+\beta^2} \quad (3)$$

$$x_n = \frac{2X_{in}}{R} = \frac{\alpha}{1+\alpha^2} + \frac{\beta}{1+\beta^2} \quad (4)$$

The voltage reflection coefficient (Γ) and voltage standing wave ratio (VSWR) are calculated as:

$$\Gamma = \frac{z_n - 2}{z_n + 2} = \frac{x_n^2 + r_n^2 - 4}{x_n^2 + (r_n+2)^2} + j\frac{4x_n}{x_n^2 + (r_n+2)^2} \quad (5)$$

$$VSWR = \frac{1+|\Gamma|}{1-|\Gamma|} \quad (6)$$

The perfect input matching for the balun will be achieved if $Z_{in} = Z_0 = Z_{unbal} = R$. To satisfy these conditions in theory, $\alpha \to \infty$ and $\beta \to \infty$, meaning that Z_{out} and L need to be as large as possible over the operating bandwidth while Z_{unbal} is designed to match with Z_o.

Using (1) to (6), Fig. 2(a) and (b) show calculated VSWR of the proposed balun with varying inductor values when Z_{out} = 130 Ω and with varying Z_{out} when L = 33 nH. It can be observed that the bandwidth of the balun (for VSWR < 2) gets wider when L and Z_{out} are higher. If L increases from 10 nH to 40 nH (Fig. 2(a)), the matching bandwidth extends from 0.3 GHz down to 0.15 GHz or the balun doubles its bandwidth ratio. The matching bandwidth at high frequency is quite constant to Z_{out} and L. In the case of varying Z_{out}, the VSWR gets smaller at high and low frequencies for larger values of Z_{out} (Fig. 2(b)).

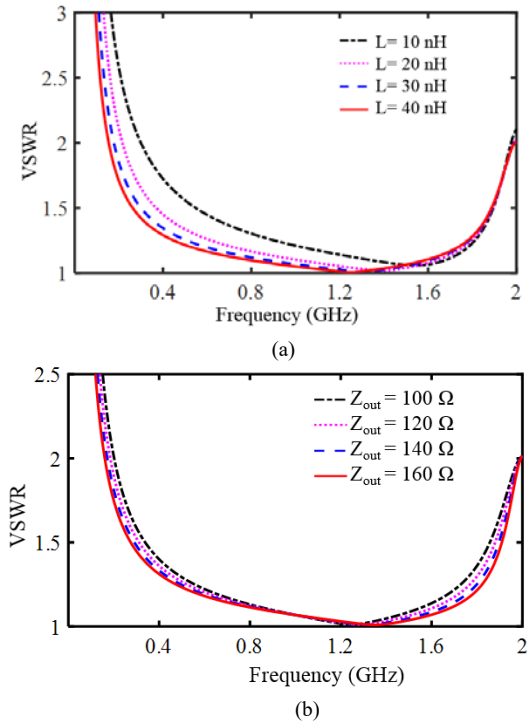

Fig. 2. Calculated VSWR of the proposed balun. (a) Z_{out} = 130 Ω and varying L. (b) L = 33 nH and varying Z_{out}.

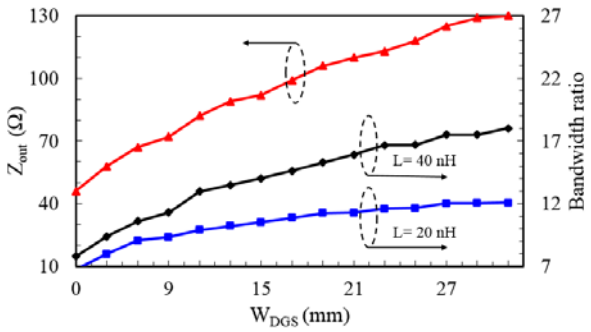

Fig. 3. Extracted characteristic impedance Z_{out} and the bandwidth ratio of the proposed balun.

To achieve a high Z_{out}, a defected ground structure (DGS) is developed in the balun. The DGS is formed by removing both the dielectric material and metal ground underneath the substrate in the vicinity of the coaxial line. Fig. 3 shows the extracted characteristic impedance of the parasitic transmission line for the DGS width using ANSYS HFSS: High Frequency Electromagnetic Field Simulation. Using the extracted characteristic impedance, Z_{out}, the simulation of the circuit model in Fig. 1(d) is conducted in Advanced Design System

(ADS) software to calculate the bandwidth ratio of the proposed balun for L = 20 nH and L = 40 nH. The bandwidth ratio (BWR) is defined as, $BWR = f_H / f_L$, where f_H is the high cutoff frequency of the balun's passband when the insertion loss is equal to 1 dB, and f_L is the low 1-dB cutoff frequency. As seen in Fig. 3, Z_{out} and BWR proportionally increase with respect to the defected area width and then saturate when W_{DGS} > 27 mm. Also, higher inductor values give larger bandwidth ratios. In summary, L and Z_{out} effectively control the matching bandwidth at low and high frequencies, respectively. To extend the high cut-off frequency f_H, the larger Z_{out} is desired by increasing the width of the defected ground structure. A higher value of inductance L could extend the low cut-off frequency f_L down to MHz ranges. The center frequency of the balun is scalable by adjusting the length of the semi-rigid coaxial cable. Noted that L and Z_{out} should be designed as large as possible to achieve wide bandwidth and to keep output signals balanced at the same time. Analysis of imbalances of the balun will be detailed in Section B.

B. *Analysis of Imbalances*

Assuming the balun circuit in Fig. 1(d) is symmetrical between Ports 2 and 3 with respect to Port 1, the transmission line Z_0 can be removed to ease of the imbalance analysis. The balun ports are all terminated with R ($Z_{bal} = Z_{unbal} = R$). From S-parameter definitions [11], [30]: $S_{21} = 2V_2/V_1$ and $S_{31} = 2V_3/V_1$, where V_1 is the source voltage at unbalanced port and V_2 and V_3 is voltage at Port 2 and Port 3, respectively. V_2 and V_3 are determined with respect to V_1 using voltage division.

$$V_2 = \frac{V_1 Z_2}{Z_1 + Z_2 + R} \quad (7) \qquad V_3 = \frac{V_1 Z_1}{Z_1 + Z_2 + R} \quad (8)$$

where $Z_1 = (j\omega L) \,//\, R$ and $Z_2 = (jZ_{out}\tan\theta) \,//\, R$. Using (7) and (8), the phase imbalance ($\Delta\phi = 180^0 - |\angle(S_{31}) - \angle(S_{21})|$) and amplitude imbalance ($\Delta A = \mathrm{dB}(|S_{31}|) - \mathrm{dB}(|S_{21}|)$) of the balun in Fig. 1 (d) can be calculated as:

$$\Delta\phi = 180^o - \left| \angle\left(\frac{2Z_1}{Z_1 + Z_2 + R}\right) - \angle\left(\frac{2Z_2}{Z_1 + Z_2 + R}\right) \right| \quad (9)$$

$$\Delta A = dB\left|\frac{2Z_1}{Z_1 + Z_2 + R}\right| - dB\left|\frac{2Z_2}{Z_1 + Z_2 + R}\right| \quad (10)$$

It can be expected from (9) and (10) that the amount of amplitude and phase imbalances converge to zero when L and Z_{out} both become very large (for which $Z_1 = Z_2 = R/2$). As a result, high values of L and Z_{out} properly reduce the imbalances of the balun at low frequencies. Fig. 4(a) shows the calculated and simulated imbalances of the balun circuit in Fig. 1(d) with varying inductor values while Z_{out} = 130 Ω at f = 0.1 GHz and f_0 = 1 GHz. The calculated results of the imbalances agree with those of circuit simulations in ADS. The inductance is determined by two criteria: input impedance matching and phase and amplitude imbalances. An infinitely large inductance could improve input impedance matching at frequency ranges below 1 GHz [Fig. 2(a)], but will drastically degrade the imbalances of the balun shown in Fig. 4 (a). Here, the minimum theoretical values of phase and amplitude imbalances are achieved with L = 33 nH, resulting in $Z_L = Z_{out}\tan(\pi f/2f_0) = 21\ \Omega$ with f_0 = 1 GHz.

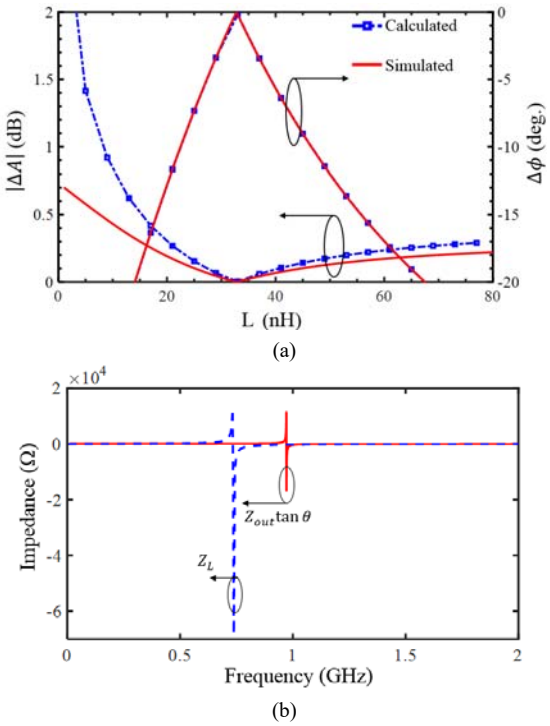

Fig. 4. (a) Calculated and simulated amplitude and phase imbalances at f = 0.1 GHz when varying inductor and Z_{out} = 130 Ω. (b) Extracted impedance from ANSYS HFSS simulations.

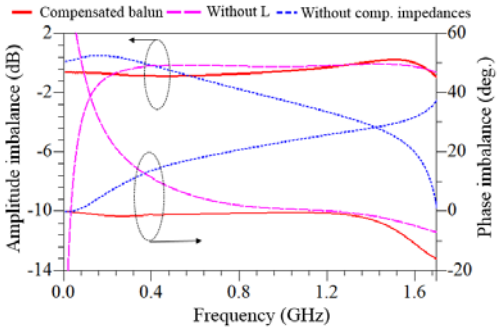

Fig. 5. Simulated imbalances of the balun without the inductor alone, without compensated impedances alone, and with inductor and compensated impedance all together using ANSYS HFSS.

The realized 35 nH spiral inductor has a simulated self-resonance frequency of 738 MHz. To achieve good balances in theory, the two output branches should satisfy the condition: $Z_L = 2\pi f_0 L_{eff} = Z_{out}\tan(\pi f/2f_0) = Z_{out}\tan\theta$. However, $Z_{out}\tan\theta$ does not align with Z_L over the entire operating band. Fig. 4(b) plots the full -wave EM simulation of impedances $Z_{out}\tan\theta$ and Z_L. Here, the HFSS simulation of the semi-rigid coaxial transmission line with an actual length over the defected ground is conducted. Then, input impedance $Z_{stub} = Z_{out}\tan\theta$ of the semi-rigid coaxial line is extracted. As seen in Fig. 4(b), the "transition frequency" of $Z_{out}\tan\theta$ is at 971 MHz. After the self-resonance frequency of the spiral

inductor at 738 MHz, the impedance differences between Z_L and $Z_{out}\tan\theta$ become large. Therefore, the additional impedances at Ports 2 and 3 are used to compensate for the phase and amplitude imbalances. These compensated impedances also reduce the effect of the discontinuity reactance created by the coaxial line to microstrip transitions. The discontinuities become significant above 1 GHz. For these reasons, the compensated impedances in a tapered structure are employed [12], [18].

The impedances (Z_{2r}, Z_{2i}, Z_{3r} and Z_{3i}) are used to compensate for the phase and amplitude imbalances when the balun is interfaced with coaxial connectors. In our design, we start with low characteristic impedance around 25 Ω because the balun is designed for 25 Ω at the balanced ports. We then tune the impedance values to get good phase and amplitude imbalances ($|\Delta\phi| < 10$ deg.) and ($|\Delta A| < 1$ dB) at high frequency (1.6 GHz). Fig. 5 shows simulated imbalances of the proposed balun with both the spiral inductor and compensated impedances at balanced ports, without the inductor, and without the compensated impedances. To have $|\Delta\phi| < 10$ (deg.) and $|\Delta A| < 1$ dB, the balun limits its operating bandwidth from 0.4 GHz to 1.6 GHz without the inductor and from 1 MHz to 0.3 GHz without using compensated impedances. In the case of a fully compensated balun, the bandwidth extends from 1 MHz to 1.6 GHz. In summary, the on-board inductor and output compensated impedances significantly improve the balances of the proposed balun over its operating bandwidth.

C. *Multiphysics Analysis of Power Handling Capabilities*

1) *Theoretical Power Handling Capability*

To analyze thermal performance of the balun under a very high power CW signal (500-1000 W), we first estimate average power handling capabilities (APHC) with respect to transmission losses and the glass transition temperature (T_g). The thermal profile on the balun depends on the heat distortion temperature of copper, the ceramic substrate material and the dielectric of the coaxial cable. Using a heat transfer analysis method [28], [29], the APHC of the proposed balun can be numerically calculated as follows,

$$P_{APHC} = \frac{T_g - T_{amb}}{\Delta T + \dfrac{\Gamma_{avg}}{2Ah_c}} \tag{11}$$

where T_{amb} is the room temperature, $2A$ is the whole top and bottom surface area of the TMM10i substrate neglecting defected substrate area (air), $h_c = 10\ \mathrm{W/m^2.^\circ C}$ is the natural convection heat transfer coefficient, ΔT is the generated temperature [24]. Γ_{avg} is the average transmission loss calculated from full-wave HFSS simulation. As expected from (11), the balun can handle the highest power when its substrate material and coaxial cable have the lowest loss and the highest glass transition temperature. Therefore, we have chosen an ultra-low loss semi-rigid coaxial cable (UT-250C-ULL) and a thermoset substrate, TMM10i that has high glass transition temperature of 590 °C, high thermal conductivity of 0.76 W/m/K and high breakdown electric strength of 2×10^6 V/m. Fig. 6 shows the calculated average power handling capability using (11) and the HFSS-simulated average insertion loss of the balun ($\mathrm{IL} = -10\log_{10}(|S_{12}|^2 + |S_{13}|^2)$ (dB)). The calculated average power handling capability of the proposed TMM10i balun is ~59.6 dBm (912 W) at 0.6 GHz and ~58.7 dBm (741 W) at 1.6 GHz and is reduced at higher frequencies as the transmission loss of the balun increases.

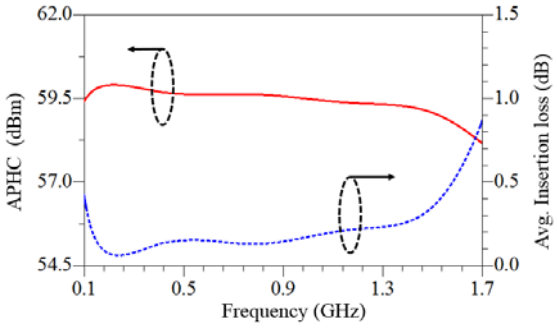

Fig. 6. Calculated average power handling capability (APHC) of the proposed balun using (11).

The peak power handling capability (PPHC) of the proposed balun is determined by the dielectric strength of the substrate, the dielectric of the connector and semi-rigid cable [26]. The electric strength of the TMM10i substrate and Teflon PTFE is on the order of 20 kV/mm and 10 kV/mm, respectively. Thus, the PPHC of the proposed balun very much depends on the electric strength of Teflon PTFE, which is the dielectric of the semi-rigid coaxial cable. The ultra-low loss coaxial cable (UT-250C-ULL) has an estimated peak power handling capability of 1482.9 W at 1 GHz.

Additionally, there are two regions of the proposed balun sensitive to a corona discharge: 1) the gap formed between the microstrip trace and top ground at the unbalanced input port where the electric strength of input signal has its maximum intensity. We have increased the critical gap for high power operation while still maintaining the balun electrical performance and 2) the dielectric between the inner and outer conductors of the semi-rigid coaxial cable. The dielectric of the cable has a low-loss tangent and a much higher dielectric strength than air (3 kV/mm). The properties of the dielectric will protect the coaxial cable against corona discharge [2].

2) *Comprehensive Multiphysics Analysis of Power Handling Capability*

We have conducted comprehensive multiphysics ANSYS analysis to determine power handling, temperature rise, local hot spot and thermal stress of the balun as a function of input power. The temperature rise and deformed mesh are fed back into an electromagnetics (EM) model to analyze the corresponding electrical changes of the proposed coaxial balun. Fig. 7 shows the temperature rise and structural deformation profiles of the proposed balun with the input power of 590 W at 0.6 GHz. In the coupled electromagnetics – thermal - structural analysis, the dielectric loss of the semi-rigid coaxial cable increases with temperature. Thus, the thermal and stress profiles will vary with the feedback temperature rise, resulting

in a converged maximum temperature of 104 °C along the cable dielectric material and 108 °C at the junction of the coaxial cable and microstrip trace near the output. Also, a maximum deformation of 0.1 mm occurs along the balun edge-sides and will not affect the balun performance over its low-frequency bandwidth below 2 GHz. Fig. 7(c) shows the equivalent (von-Mises) stress profiles of the proposed balun. The thermal stress mostly happens at the inner conductor to the microstrip interface and output balance ports. Along the TMM10i substrate, the Von-mises stress is 175 MPa, which is below the material yield strength limit (280 MPa).

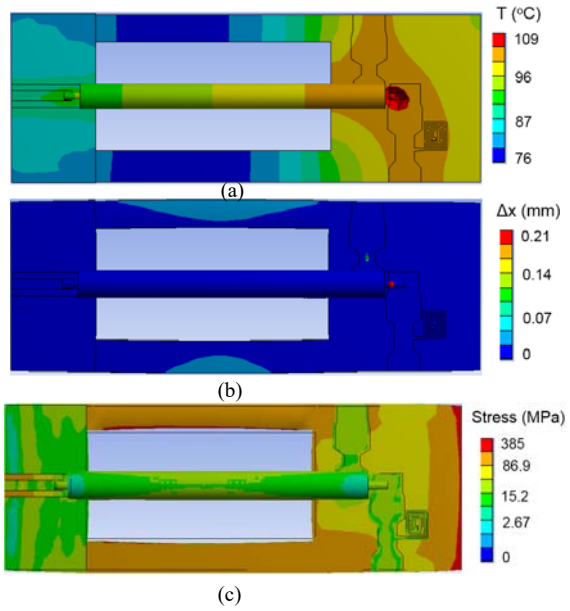

Fig. 7. Coaxial balun with 590 W input power at 0.6 GHz. (a) Temperature rise profile. (b) 3-D deformation distribution. (c) 3-D thermal stress.

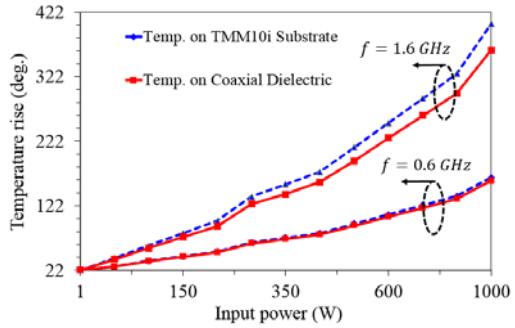

Fig. 8. Temperature rise profile on the substrate and coaxial dielectric material of the proposed balun using multiphysics ANSYS simulations.

Fig. 8 shows the maximum temperature rise in the TMM10i substrate and the dielectric material of the semi-rigid coaxial cable. Because the coaxial dielectric material (low-density PTFE) has a glass transition temperature of $T_o = 262$ °C, the balun can handle up to 670 W at 1.6 GHz and more than 1000 W at 0.6 GHz. The EM model of the balun updates the feedback deformed mesh at different power levels and provides simulated power-dependent S-parameters to verify electrical performance. Fig. 9 shows a full-wave EM simulation with the input power of 1 W and 600 W for comparison. It can be seen that there is an expected frequency shift of 19 MHz with $P_{in} =$ 600 W. The reference frequency is the lowest frequency ($f =$ 0.1 GHz) at 1 Watt input power.

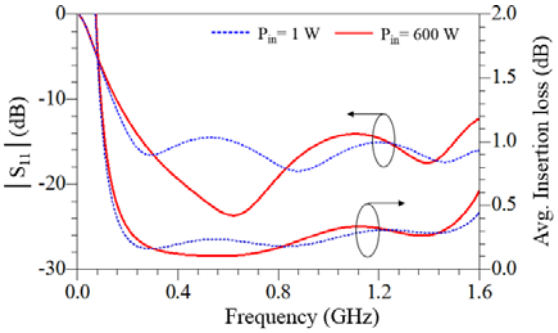

Fig. 9. Return loss and insertion loss of the proposed balun with the input power of 1 W and 600 W.

III. Electrical and High Power Measurements

A. Realization of the High Power and Ultra-wideband Balun

We have designed and fabricated the proposed high power and wide bandwidth balun to achieve a bandwidth ratio of higher than 15 at a center frequency $f_0 = 1$ GHz. The unbalanced port and balanced port impedances are chosen as $Z_{unbal} = 50\ \Omega$ and $Z_{bal} = 25\ \Omega$, respectively. The calculated circuit parameters are given as $L = 35$ nH, $W_{DGS} = 30$ mm and $Z_{out} = 130\ \Omega$. The designed spiral inductor [Fig. 1(b)] includes three turns with $l_1 = 7$ mm, $l_2 = 5.5$ mm, $w = 0.45$ mm, and $s = 0.45$ mm. The balun is fabricated on a Rogers TMM10i substrate with a dielectric constant (ε_r) of 9.8 and a thickness (h) of 2.54 mm. Table I summarizes the final dimension values of each impedance. Fig. 10 shows the connectorized balun prototype with the size of 116 mm x 47 mm x 2.54 mm.

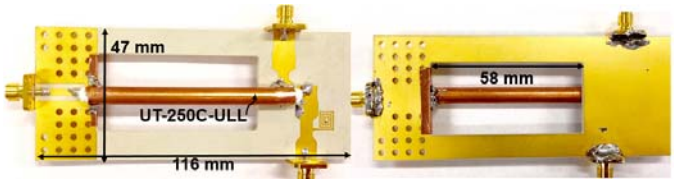

Fig. 10. Prototype of the ferriteless balun. (a) Top view. (b) Bottom view.

TABLE I
IMPEDANCE DESIGN SUMMARY

Parameter	R	$R/2$	Z_{2i}	Z_{2r}	Z_{3i}	Z_{3r}
Impedance (Ω)	50	25	19	28	26	19
Microstrip width (mm)	2.54	7.9	8.8	3.9	4.7	8.8
Microstrip length (mm)	15	6	5	2.6	2.8	5

B. Electrical Measurements

Three test ports (Ports 1, 2 and 3) of the four-port network analyzer (PNA-X N5247A) were used to evaluate the small-signal electrical performance of the balun. Guided Short-Open-Load-Thru (SOLT) multiport calibration available from the Keysight PNA-X N5247A was performed for three ports using coaxial standards. In the 3-port calibration, each test port was connected to the Short standard, Open standard and Load standard. Then, a Thru standard connection was made between port pairs (Ports 1 and 2, Ports 1 and 3).

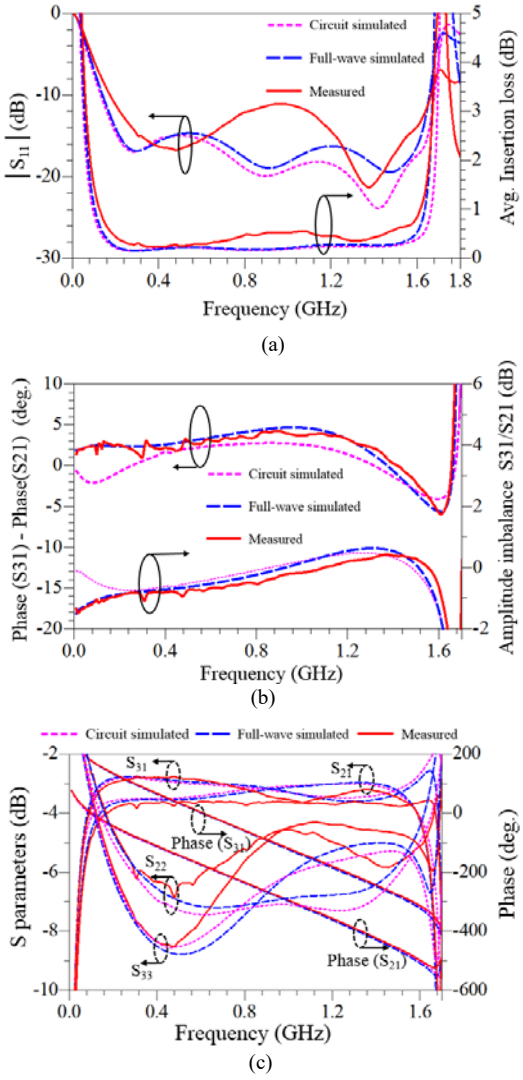

Fig. 11. Measured results of the balun. (a) Return losses and average insertion losses. (b) Phase and amplitude imbalances (c) |S22|, |S33|, |S21|, |S31|, phase (S21), and phase (S31).

Fig. 11 shows the measured, full-wave simulated, and circuit simulated return losses, average insertion losses, and phase and amplitude imbalances of the balun. The circuit simulation uses an ADS microstrip model of the rectangular spiral inductor that includes the self-resonance behavior. It can be observed that the circuit model and full-wave simulations can predict the trend of the balun performance well. The return loss of the balun is better than 10 dB from 0.1 GHz to beyond 1.6 GHz. The balun achieves a measured average insertion loss of less than 1 dB from 0.1 GHz to 1.6 GHz. Fig. 11 (b) shows that a measured phase difference of ±5° is achieved from 10 MHz to greater than 1.6 GHz and an amplitude imbalance of less than ±0.5 dB and ±1 dB is well maintained from 650 MHz to 1.6 GHz and from 30 MHz to 1.6 GHz, respectively. Fig. 11(c) shows a good agreement between simulation and measurement of the |S22|, |S33|, |S21|, |S31|, phase (S21), and phase (S31).

C. High Power Handling Measurement

We have conducted the measurements of the balun prototype with high power input signals. Fig. 12 shows the block diagram set-up of the high power measurements. The test set-up includes a 600 W tube amplifier, high power hybrid couplers, 40 dB attenuators, and a thermal infrared camera (FLIR S65-H5) to capture the relative temperature rise profile in the balun. A CW signal has been applied to the balun at ambient pressure (p = 1000 mbar) and temperature (T_{amb} = 22 °C) and was swept over frequency and power ranges. For each frequency, the test system recorded the incident power (P_1) and transmitted power (P_2 and P_3) and took an infrared image of the balun at the same time. Then, the average insertion loss (avg. IL) of the balun is calculated by,

$$IL_{\text{avg. IL}} = -10\log_{10}\left(2\sqrt{\frac{P_2P_3}{P_1^2}}\right) \quad (12)$$

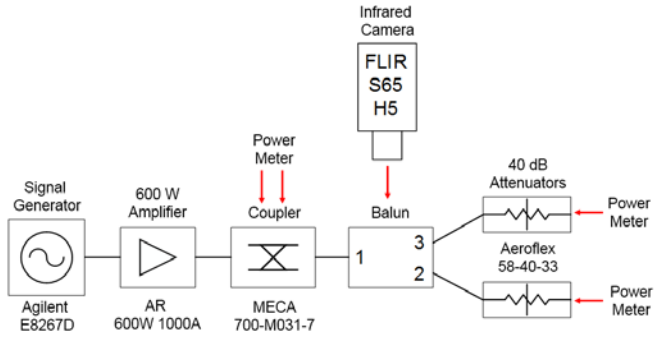

Fig. 12. High power test set-up.

Fig. 13 shows the measured temperature distribution on the balun for 350 W and 590 W input signals at 600 MHz. As compared with the simulated temperature rise profile (Fig. 7(a)), the maximum hot spot can be clearly identified close to the input and output coaxial junctions as well as at the on-board inductor with P_{in}=600 W at 600 MHz, measured T_{max} =100 °C compared with simulated T_{max}= 109 °C. The difference can be due to the ambient temperature around the balun and no heat sink being considered for the high power measurement. In short, the simulated temperature correlates with that obtained from measurements.

Fig. 14 shows the measured average insertion losses of the balun with a varying input power at different frequencies. The measured average insertion loss (IL) is calculated from the measured data from power sensors using (12). It can be observed that the measured average insertion losses remain

constant over the input power range. Compared with Fig. 11(a), the insertion loss is ~0.1 dB higher because of using three N-type connectors and adapters for high power measurement.

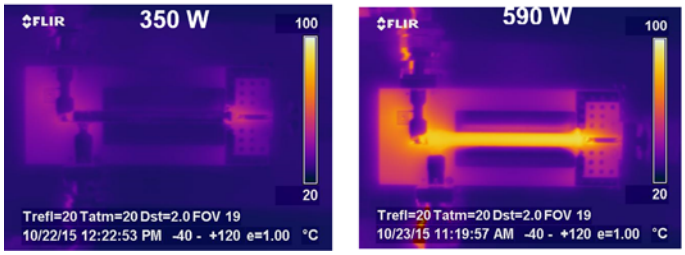

Fig. 13. Measured infrared image at 600 MHz with input power. (a) 350 W and (b) 590 W.

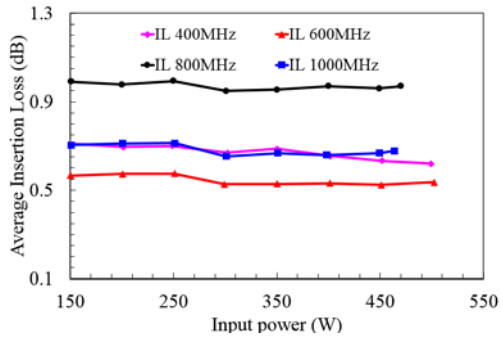

Fig. 14. Measured averaged insertion loss under varied input power.

Table II compares the proposed balun with other reported broadband high power baluns with an average insertion loss of 1 dB. Compared to published ferriteless baluns, our proposed balun has the combined highest power handling and bandwidth ratio.

TABLE II
COMPARISON OF HIGH POWER BALUN DESIGN

Design	Frequency (GHz)	Amplitude (dB) / Phase Imbalance (°)	Size in λ_g @ f_0	Topology/Power handling (P)
[3]	1-2	1/10	0.2 x 0.25	Ferriteless, P< 500 W
[4]	0.45-0.76	1/10	0.2 x 0.25	Ferriteless, P< 700 W
[6]	0.05-2.3	1/8	0.19 x 0.28	Coupled-line, P < 10 W
[9]	0.08-1.86	0.4/10	0.22 x 0.22	Coupled-line, P <15 W
[10]	1-9	1/8	0.1 x 0.06	Coupled-line, P< 15 W
[17]	0.1-1	1/10	0.16 x 0.27	Ferriteless, P< 40 W
[19]	0.1-2.8	0.3/0.6	0.1 x 0.06	Coupled-coil, P < 80 W
[22]	0.01-0.5	1/10	0.1 x 0.05	Ferrite, P < 100 W
This work	0.1-1.6	1 /5	0.12 x 0.29	Ferriteless, P> 600 W

IV. CONCLUSIONS

In this paper, the design and development of an ultra-wideband balun for high power microwave applications have been demonstrated. The multiphysics simulations are employed to design the balun in terms of high power, electrical responses, and structural integrity. A ferriteless coaxial balun model is designed and prototyped using only one quarter-wavelength coaxial section and defected ground structures to achieve a bandwidth ratio of 16:1. Our experimental results show that the proposed balun can handle up to 600 W input power. To the best of our knowledge, the proposed balun achieves the highest combined power handling and bandwidth ratio.

ACKNOWLEDGMENT

This work is supported by Raytheon Company.

REFERENCES

[1] G. N. Saddik, R. S. Singh, and E. R. Brown, "Ultra-wideband multifunctional communications/radar system," *IEEE Trans. Microw. Theory Techn.*, vol. 55, pp. 1431-1437, July 2007.

[2] K. Shamsaifar, T. Rodriguez, and J. Haas, "High-power combline diplexer for space," *IEEE Trans. Microw. Theory Techn.*, vol. 61, pp. 1850-1860, Apr. 2013.

[3] A. Maekawa, T. Yamamoto, E. Mitani, and S. Sano, "A 500 W push-pull AlGaN/GaN HEMT amplifier for L-band high power application," *IEEE MTT-S Int. Microw. Symp. Dig.*, June 2006, pp. 722-725.

[4] J. He, J. H. Qureshi, W. Sneijers, D. A. Calvillo-Cortes, and L. C. N. de Vreede, "A wideband 700W push-pull Doherty amplifier," in *IEEE MTT-S Int. Microw. Symp. Dig.*, July 2015, pp.1-4.

[5] N. Marchand, "Transmission line conversion transformers," *Electronics*, vol. 17, no.12, pp. 142-145, Dec. 1944.

[6] C. V. Pham, B. Pham, A. -V. Pham, and R. E. Leoni, "A 46:1 bandwidth ratio balun on multilayer organic substrate," in *IEEE MTT-S Int. Microw. Symp. Dig.*, July 2015, pp. 1-3.

[7] A. C. Chen, A. -V. Pham, and R. E. Leoni, III, "A novel broadband even-mode matching network for Marchand baluns," *IEEE Trans. Microw. Theory Techn.*, vol. 57, pp. 2973-2980, Oct. 2009.

[8] A. C. Chen, A. -V. Pham, and R. E. Leoni, III, "Development of low-loss broad-band planar baluns using multilayered organic thin films," *IEEE Trans. Microw. Theory Techn.,* vol. 53, pp. 3648-3655, Nov. 2005.

[9] B. L. Pham, H. H. Ta, A. -V. Pham, R. E. Leoni, and Y. Leviatan, "23:1 bandwidth ratio quasi-lumped component balun on a multilayer organic substrate," *IET Microw., Antennas Propag.,* vol. 10, pp. 561-567, Apr. 2016.

[10] H. H. Ta, B. L Pham, and A.-V. Pham, "Compact wide bandwidth balun based on modified asymmetric broadside coupled lines," *IEEE Microw. Wireless Compon. Lett.*, vol. 22, pp. 624-626, Nov. 2012.

[11] R. Phromloungsri, M. Chongcheawchamnan, and I. D. Robertson, "Inductively compensated parallel coupled microstrip lines and their applications," *IEEE Trans. Microw. Theory Techn.,* vol. 54, pp. 3571-3582, Aug. 2006.

[12] R. Chadha and K. C. Gupta, "Compensation of discontinuities in planar transmission lines," *IEEE Trans. Microw. Theory Techn.,* vol. 30, no. 12, pp. 2151-2156, Dec. 1982.

[13] H. R. Phelan, "A wide-band parallel-connected balun," *IEEE Trans. Microw. Theory Techn.,* vol. 18, pp. 259-263, May 1970.

[14] W. K. Roberts, "A new wide-band balun," *Proc. IRE,* vol. 45, pp. 1628-1631, Dec. 1957.

[15] R. Bawer and J.J. Wolfe, "A printed circuit balun for use with spiral antennas," *IRE Trans. Microw. Theory Techn.,* vol. 8, pp. 319-325, May 1960.

[16] D. A. Dunn, J. W. McLaughlin, and R. W. Grow, "A wide-band balun," *IRE Trans. Microw. Theory Techn.,* vol. 6, pp. 314-316, July 1958.

[17] R. M. Smith, J. Lees, P. J. Tasker, J. Benedikt, and S. C. Cripps, "A 40W push-pull power amplifier for high efficiency, decade bandwidth applications at microwave frequencies," in *IEEE MTT-S Int. Microw. Symp. Dig.,* Aug. 2012, pp. 1-3.

[18] G. Oltman, "The compensated balun," *IEEE Trans. Microw. Theory Techn.,* vol. 14, no. 3, pp. 112-119, Mar. 1966.

[19] Johannes Horn and G. Boeck, "Ultra-wideband balun for power applications," in *Proc. 34th European Microw. Conf. (EuMC),* Apr. 2004, pp. 369-371.

[20] G. A. Hofbauer, "An ultra-wideband microwave balun using a tapered coaxial coil structure working from kHz range to beyond 26.5 GHz," in *IEEE MTT-S Int. Microw. Symp. Dig.*, Oct. 2005, pp. 551-554.

[21] A. K. Ezzeddine and H. C. Huang, "10W ultra-broadband power amplifier," in *IEEE MTT-S Int. Microw. Symp. Dig.*, Sept. 2008, pp. 643-646.

[22] J. Cho *et al*., "Design of a 100watt high-efficiency power amplifier for the 10-500MHz band," in *Proc. IEEE Asia Pacific Microw. Conf. (APMC)*, Jan. 2009, pp.285-288.

[23] H. Noto, K. Yamauchi, M. Nakayama, M. Kohama, and Y. Hirano, "A broadband 200W GaN push-pull power amplifier enhanced second harmonic suppression with point-symmetric 2-stage baluns," in *Proc. European Microw. Integr. Circuits Conf. (EuMIC)*, Oct. 2011, pp. 252-255.

[24] I. Bahl and K. Gupta, “Average power-handling capability of microstrip lines,” *IEE J. Microw. Opt. Acoust.,* vol. 3, no. 1, pp. 1–4, Jan. 1979, UK.

[25] *Transformers/Baluns*, M/A-COM Inc., 2016. [Online]. Available: www.macom.com/products/passives/transformers--baluns

[26] M. A. Sánchez-Soriano, M. Edwards, Y. Quéré, D. Andersson, S. Cadiou and C. Quendo, "Multiphysics study of RF/microwave planar devices: Effect of the input signal power," in *Proc. 15th Int. Conf. on Thermal, Mech. and Multiphysics simulation and experiments in Microelectron. and Microsyst. (EuroSimE)*, May 2014, pp. 1-7.

[27] H. H. J. M. Janssen, E. J. W. t. Maten, and D. v. Houwelingen, "Simulation of coupled electromagnetic and heat dissipation problems," *IEEE Trans. Magn.,* vol. 30, pp. 3331-3334, Sept. 1994.

[28] Y. J. Cheng, K. Wu, and W. Hong, "Power handling capability of substrate integrated waveguide interconnects and related transmission line systems," *IEEE Trans. Adv. Packag.*, vol. 31, pp. 900-909, Aug. 2008.

[29] M. Á Sánchez-Soriano, Y. Queré, V. Le Saux, C. Quendo and S. Cadiou, "Average power handling capability of microstrip passive circuits considering metal housing and environment conditions," *IEEE Trans. Compon. Packag. Manuf. Technol.,* vol. 4, pp. 1624-1633, Oct. 2014.

[30] D. M. Pozar, Microwave Engineering, 2nd ed. Hoboken, NJ: Wiley,1998.